

Article

A Dynamic Propagation Numerical Model of Hydraulic Fracture Interactions with Pre-Existing Complex Natural Fractures

Shuangming Li ¹, Huan Zhao ^{1,2,*}, Jianbo Wang ² , Xiaorui Xie ², Lan Qin ³, Linhao Zou ² and Yapeng Liu ²

¹ State Key Laboratory of Shale Oil and Gas Enrichment Mechanisms and Effective Development, Beijing 102206, China

² College of Petroleum Engineering, Northeast Petroleum University, Daqing 163318, China

³ Petrochina Southwest Oil and Gas Field Company, Chengdu 610051, China

* Correspondence: zhaohuan@nepu.edu.cn

Abstract: The propagation of hydraulic fractures is highly influenced by the geological structure of the reservoir in unconventional reservoirs, such as natural fractures. In this paper, a new fluid–solid coupling dynamic model was built which presents the failure mechanism of hydraulic fracture with pre-existing simple and complex natural fractures. The cohesive element method and the maximum principal stress fracture criterion were used in the new model. An analysis was conducted to investigate the impact of various factors, including encounter angle, in situ stress, elastic modulus, and Poisson’s ratio, on the propagation of hydraulic fractures. The simulation results indicate that the encounter angle and the in situ stress are the main factors affecting the fracture morphology. When the encounter angle and the in situ stress difference are small, hydraulic fractures propagate along natural fractures. When the elastic modulus is small, it is advantageous for the advancement of both hydraulic and natural fractures. The Poisson’s ratio has a slight effect on the fracture propagation pattern.

Keywords: hydraulic fracture; complex natural fracture; propagation mechanism; fracture morphology; rock mechanics parameters



Citation: Li, S.; Zhao, H.; Wang, J.; Xie, X.; Qin, L.; Zou, L.; Liu, Y. A Dynamic Propagation Numerical Model of Hydraulic Fracture Interactions with Pre-Existing Complex Natural Fractures. *Processes* **2024**, *12*, 899. <https://doi.org/10.3390/pr12050899>

Academic Editor: Chuanliang Yan

Received: 12 March 2024

Revised: 20 April 2024

Accepted: 25 April 2024

Published: 28 April 2024



Copyright: © 2024 by the authors. Licensee MDPI, Basel, Switzerland. This article is an open access article distributed under the terms and conditions of the Creative Commons Attribution (CC BY) license (<https://creativecommons.org/licenses/by/4.0/>).

1. Introduction

Unconventional oil and gas reservoirs rely significantly on natural fractures for their development, making them essential and crucial. Natural fractures cause branch fractures during hydraulic fracture operation. Complex fracture networks are formed during the use of hydraulic fracture technology in unconventional oil and gas reservoirs through hydraulic fractures interacting with pre-existing complex natural fractures. This technology can increase the stimulation reservoir volume and greatly enhance oil and gas recovery [1–3]. There are different sizes of natural fractures which have uneven distribution and intricate complexity in underground rocks due to the complex geological structure. A massive number of natural fractures or closed fractures, which are the weak surface of hydraulic fracture propagation, are sealed by precipitation cements [4]. Natural fractures have influence on the hydraulic fracture propagation, which has prompted many researchers to set up a variety of propagation criteria. The research methods include theoretical research, physical model experiment and numerical simulation [5,6].

The propagation of hydraulic fractures within rocks, specifically the mechanics behind the critical propagation of preset fractures, poses a significant challenge [7]. In 1913, Inglis conducted a stress analysis of the uniform stress in a flat elliptical hole [8]. Based on this research, Griffith laid a solid foundation for the universal theory of fracture through the concept of energy balance and the defect hypothesis. Contemporary fracture mechanics are based on Griffith’s concept of energy balance. The stress intensity factor at the fracture tip serves as a fundamental parameter for describing the initiation and propagation of fractures triggered by hydraulic fracturing, utilizing the principles of fracture mechanics [9,10]. Ayatollahi [11] proposed the maximum tangential strain energy density criterion for brittle

fracture considering the I/II/III mixed mode. Yao et al. [12] established an energy-based analysis method based on the Griffith stability criterion to predict the influence of natural fractures on hydraulic fracture propagation. Deng et al. [13] studied the influence of the original rock stress on the fracture behavior of a single fracture based on the stress intensity factor criterion, but did not consider the influence of the presence of natural fractures on fracture initiation and expansion. Zhang et al. [14] analyzed the influence of displacement and stress difference on hydraulic fracturing fracture propagation by carrying out large-scale true triaxial tests on shale outbursts containing natural fractures. Hou et al. [15] carried out true triaxial hydraulic fracturing material model experiments on tight limestone outcroppings, and analyzed the influence of in situ stress difference, fracturing fluid viscosity, variable displacement, acid treatment and other factors on fracture propagation law. Gang Hui et al. [16] proposed an unconventional fracture model based on experimental and well-logging data, and considered the interaction between subsurface fractures and natural fractures influenced by fluid flow and rock mechanics. Swapnil Kar et al. [17] analyzed the effective permeability of reservoirs under different fracturing conditions by comparing the displacement field and stress field after hydraulic fracture simulation. However, quantifying the propagation pattern when hydraulic fractures interact with intricate pre-existing natural fractures remains challenging.

Currently, several noteworthy studies have explored the interactions between hydraulic fractures and natural fractures using the displacement discontinuity method (DDM) by incorporating contact forces between particles. DDM theory, which can be used to simulate nonlinear processes such as rock fracture, was proposed by Cundall, who overcame the continuity assumption in continuum mechanics [18]. Cottrell [19] established a numerical model of a discrete fracture network and investigated a hydraulic fracture interacting with single pre-existing natural fractures using DDM. Xia et al. [20] developed a two-dimensional model of single fracture propagation by using the discrete element numerical simulation method and analyzed the influence of the stress shadow effect on fracture propagation direction. Fatahi [21] investigated the mechanisms of hydraulic fracture interacting with pre-existing natural fractures using DDM and experimental studies. Song et al. [22] used ABAQUS to establish a fracture reservoir model and a bilinear traction–separation on-tological model to describe the process of fracture initiation and extension. Rueda et al. [23] investigated the effect of prefabricated fractures on hydraulic fracture extension based on the discrete element method of hydrodynamics. However, the basic assumption of the DDM is linear elastic fracture mechanics (LEFM), which is only applicable to brittle rocks. This method is limited in its application to quasi-brittle/ductile rocks.

The intersection and expansion of hydraulic fractures and natural fractures cannot truly be reflected by the traditional stimulation method. To address the aforementioned constraints, numerous scholars have embraced the cohesive zone method (CZM) for modeling the commencement and advancement of fractures. CZM simulates natural fractures by embedding zero-thickness cohesive elements, avoiding the singularity of fracture tip and predicting the propagation of hydraulic fractures and natural fractures in a more realistic way. In this study, by utilizing the cohesive zone method, the dynamic propagation model of hydraulic fracture interacting with the pre-existing complex natural fracture was established, combining the maximum principal stress fracture criterion, and then the influence factors of fracture morphology and propagation law were analyzed. This study offers technical insights that can guide the development of unconventional reservoirs.

2. Mechanical Parameter Experiment

The tight sandstone reservoir has similar geological characteristics to shale, such as low permeability, low porosity, strong heterogeneity, etc. Volume-fracturing technology has become an effective measure to exploit tight sandstone reservoirs. Rock mechanics parameters are the parameters that characterize the basic characteristics of rocks. This experimental device adopts the triaxial rock mechanics test system introduced by the Phenix Company in the United States to conduct a uniaxial compression test and a triaxial

compression test. The rock core sample is as shown in Figure 1. The size of the rock samples for rock mechanical testing was $\Phi 25 \times 50$ mm, and the experiment on the rock physical and mechanical properties of Block X was carried out.



Figure 1. Tight sandstone core samples.

The uniaxial compression test is conducted by directly adding axial load without peripheral pressure and pore pressure, and controlling the loading with the strain or stress rate until the rock sample is destroyed. Triaxial compression tests simulate horizontal stress, pore pressure and temperature under stratigraphic conditions, and the strain or stress loading rate is controlled according to the characteristics of the rock samples tested and the experimental requirements. As shown in Table 1, the elastic modulus of Block X ranges from 18.99 GPa to 22.50 GPa, and the Poisson's ratio ranges from 0.19 to 0.30.

Table 1. The results of the rock mechanics test.

Well Number	Rock Sample Number	Pressurization (MPa)	Elastic Modulus (GPa)	Poisson's Ratio	Shear Modulus of Elasticity (GPa)	Bulk Modulus (GPa)
W1	1-1	0	12.40	0.19	5.21	6.67
	1-2	14.4	18.19	0.23	8.14	7.91
	1-3	30	19.50	0.19	8.89	8.06
W2	2-1	0	10.99	0.30	4.21	9.34
	2-2	16.6	19.98	0.26	8.85	8.98
	2-3	40	22.50	0.21	10.18	9.49

3. Mathematical Models

3.1. Fluid-Structure Coupling Mechanism

To simulate the propagation of hydraulic fractures intersecting with intricate pre-existing natural fractures, a model was developed through the integration of various processes, including fracture propagation, fluid dynamics within the fractures, deformation of the surrounding rock and fluid loss in porous media. The mechanical response of porous materials is described by the theory of pore elasticity, which shows explicit coupling between the expansion of the matrix skeleton and the pressure of the diffused pore fluid. The total stress can be expressed in terms of effective stress and pore pressure [24],

$$\sigma_{ij} = \sigma'_{ij} + \alpha p \delta_{ij} \quad (1)$$

where σ_{ij} is the total stress, MPa. σ'_{ij} is the effective stress, MPa. p is the pore pressure, MPa. α is the Biot constant, 0.75. δ_{ij} is the Kronecker delta.

For the linear elastic case, the constitutive relationship can be expressed by the effective stress and the strain, as follows,

$$d\varepsilon = De : d\sigma' \quad (2)$$

According to the mass balance of the fluid, a portion of the injected fluid will fill the fracture within a certain period of time, and the remaining fluid will leak into the rock matrix of the fracture, as shown in the following equation.

$$\frac{\partial d}{\partial t} + \nabla \cdot q + (q_t + q_b) = q_{inj}\delta(x, y) \quad (3)$$

Therefore, the governing equations of the rock matrix consist of the coupled equations for fluid flow and rock deformation.

$$\sigma_{ij} - \sigma_{ij}^0 = \frac{E}{1 + \nu} \left(\varepsilon_{ij} + \frac{\nu}{1 - 2\nu} \varepsilon_{kk} \delta_{ij} \right) - \alpha (p_w - p_w^0) \delta_{ij} \quad (4)$$

3.2. Rock Failure Criteria

In this study, CZM was used to establish the model of the propagation of hydraulic fracture intersecting with pre-existing complex natural fractures. The predefined path composed of cohesive elements was embedded into the rock. This method can be used to predict the initiation and propagation of fluid pressure cracks in any joint geometry.

A bilinear constitutive model can be used to simulate the fracture process of brittle materials [25]. Damage begins when the square ratio of the nominal stresses in all directions equals 1. The criterion can be expressed as follows:

$$\left\{ \frac{\langle t_n \rangle}{t_n^0} \right\}^2 + \left\{ \frac{t_s}{t_s^0} \right\}^2 + \left\{ \frac{t_t}{t_t^0} \right\}^2 = 1 \quad (5)$$

where t_n^0, t_s^0, t_t^0 are the peak values of the nominal stress when the deformation is normal compared to the interface, in the first, and in the second shear direction, respectively. Figure 2 shows the criteria for damage assessment in Cohesive Elastic–Plastic elements.

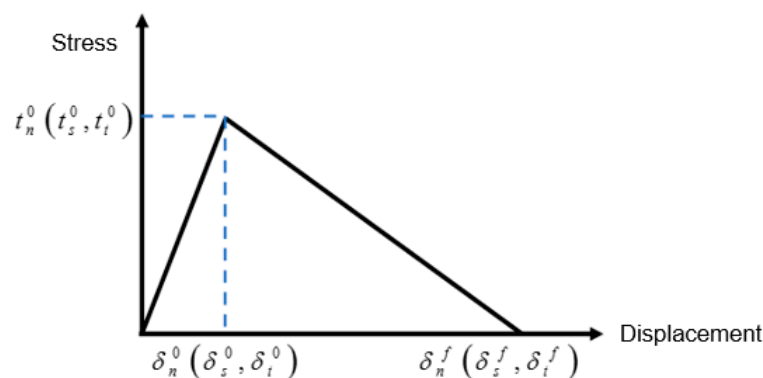


Figure 2. Bilinear constitutive model.

3.3. Fluid Flow within Fractures

Assuming that the fracturing fluid behaves as an incompressible Newton fluid, the fluid flow within the cohesive unit can be categorized into two distinct flows: tangential and normal. The normal flow pertains to the leakage of fracturing fluid into the formation, whereas the tangential flow serves as the driving force for fracture propagation [26]. Figure 3 illustrates the flow pattern of the fracturing fluid within the fracture.

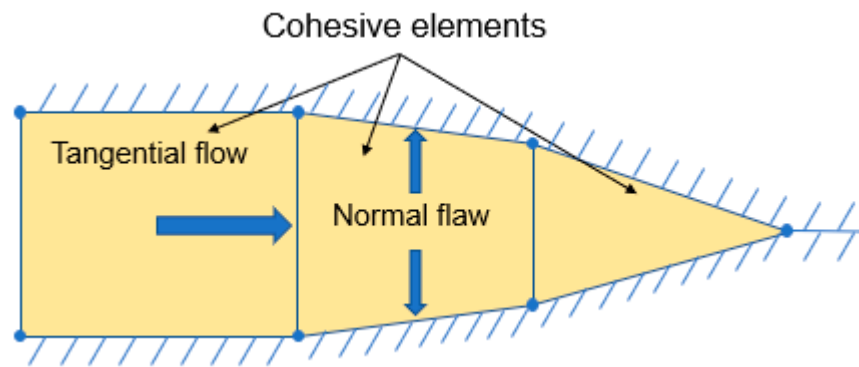


Figure 3. Fluid flow model in a cohesive unit.

Fluid flow within the fracture satisfies the cubic law [27],

$$\mathbf{q}d = -\frac{d^3}{12\mu} \nabla p \quad (6)$$

where \mathbf{q} is the volume rate of flow through a cross-section of the fracture, and d is the fracture width, which varies constantly. ∇p is the fluid pressure gradient along the cohesive zone. μ is the viscosity of the fracturing fluid.

Normal flow within the fracture is based on the following principles,

$$\begin{cases} q_t = c_t(p_i - p_t) \\ q_b = c_b(p_i - p_b) \end{cases} \quad (7)$$

where q_t and q_b represent the velocity of fluid flow into the upper and lower surfaces of the cohesive unit, and c_t and c_b define the corresponding fluid leak-off coefficients of the upper surface and the lower surface, respectively. p_i is the pressure interpolated through the virtual node in the cohesive cell, and p_t and p_b are the fluid pressure on the upper and lower surfaces of the cohesive element, respectively.

3.4. Numerical Model

Hydraulic fracture propagation is complicated as hydraulic fractures interact with pre-existing complex natural fractures. The propagation path is determined by the stress distribution near the intersecting point and the features of natural fractures [28,29]. There are four types of two-fracture intersections in the two-dimensional category: (1) hydraulic fracture (HF) propagation in the original direction, without the influence of natural fracture (NF), (2) hydraulic fractures which stop spreading and are blocked by natural fractures, (3) hydraulic fractures which extend along one side of the natural fractures and (4) hydraulic fractures which flow along both sides of the NF. The possible pathways due to a hydraulic fracture interacting with a pre-existing natural fracture are shown in Figure 4.

The dynamic propagation numerical simulation model of interaction between hydraulic fractures and existing natural fractures is established. The model data were derived from rock mechanics parameters' experimental data in block X. It is assumed that the fracturing fluid is an incompressible Newtonian fluid and the injection rate is constant. Due to hydraulic fracturing, expansion is a symmetrical model, and a 1/2 model is established with the model size of 20 m × 20 m. The perforation position is the boundary center, and the maximum horizontal principal stress is vertical. The rock properties and storage characteristics are shown in Table 2. The pore fluid (CPE4P) mesh was used for the solid part, and the cohesive element (COH2D4P) mesh was used for the fractures considering infiltration. The fracture intersection area was locally encrypted, and 16,782 grids were divided. The grid model is shown in Figure 5, the injection pressure variation diagram is shown in Figure 6, and the schematic diagram of the model result is shown in Figure 7.

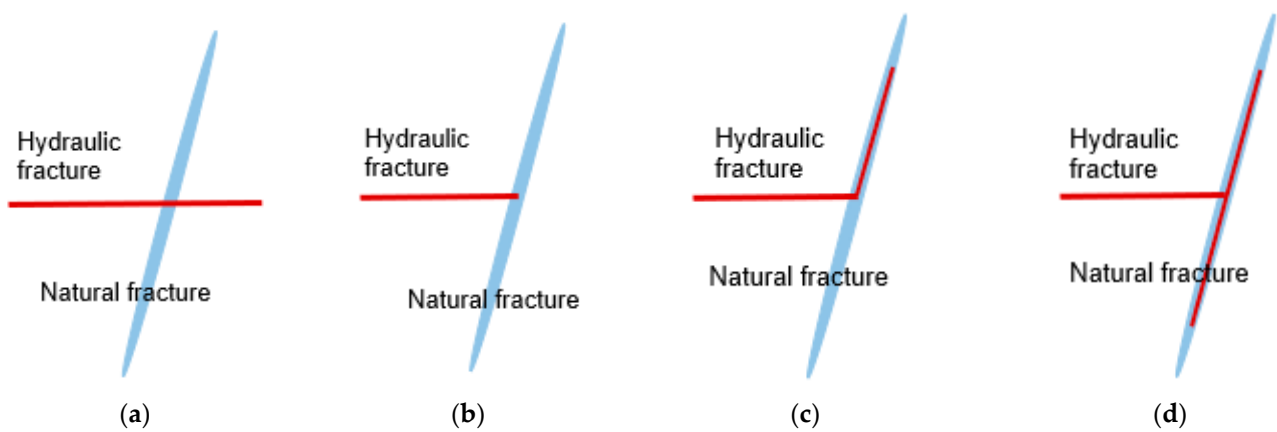


Figure 4. Possible pathways due to a hydraulic fracture (HF) interacting with a natural fracture (NF). (a) Across; (b) arrest; (c) diversion along one side of NF; (d) diversion along both sides of NF.

Table 2. Parameters of the intersection model of hydraulic fracture and natural fracture.

Parameters	Value	Parameters	Value
Depth (m)	1648	Minimum horizontal principal stress (MPa)	27
Elastic modulus (GPa)	22	Tensile strength of rock (MPa)	4.8
Poisson's ratio	0.3	Rock density (kg/m^3)	2300
Formation pressure (MPa)	17	Injection rate (m^3/min)	6
Maximum horizontal principal stress (MPa)	30	Fracturing fluid viscosity ($\text{mPa}\cdot\text{s}$)	100

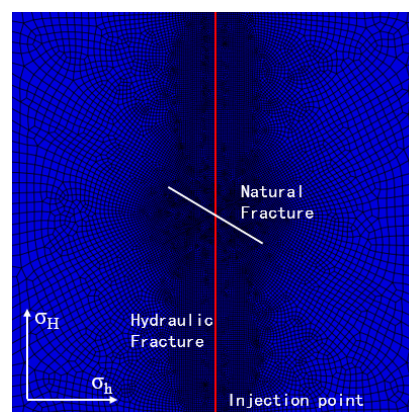


Figure 5. Model meshing.

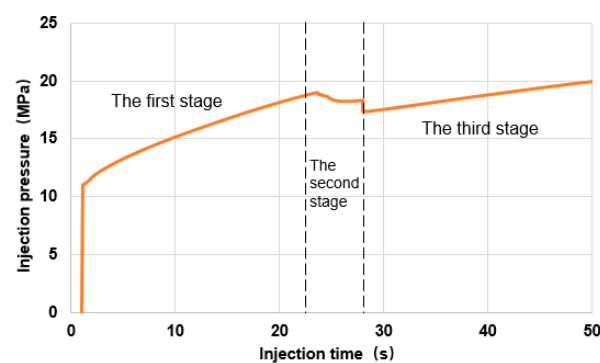


Figure 6. Injection pressure curve.

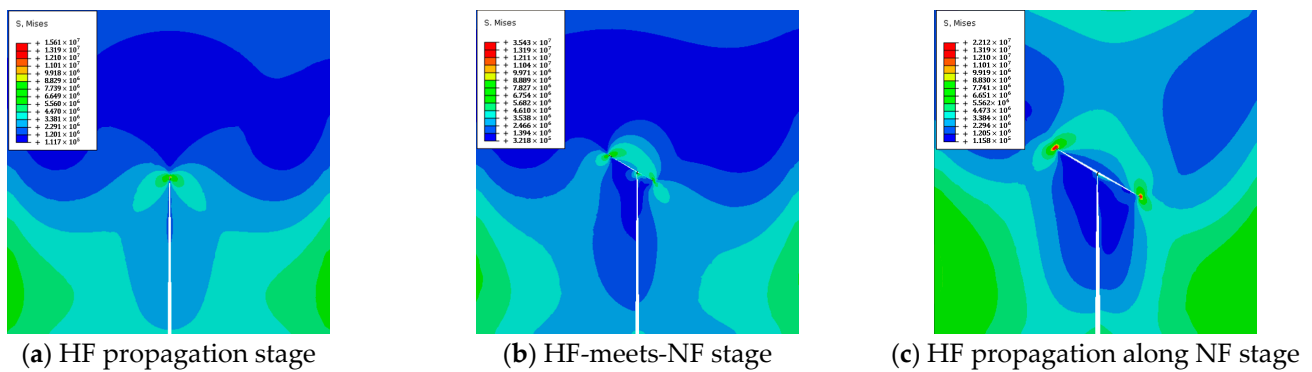


Figure 7. The stress field distributions in different propagation stages.

The dynamic propagation model shows that the propagation stage of hydraulic fracturing includes three types of propagation [30]. In the HF propagation stage, the stress concentration zone is formed at the tip of the hydraulic fracture, with an obvious plastic zone. The injection pressure increases. In the HF-meets-NF stage, it may pass through directly, extend along the natural fracture and be blocked by the natural fracture. In this model, when the hydraulic fracture intersects with the natural fracture, the natural fracture initiates to propagate and the injection pressure drops. During propagation along the NF stage, the stress concentration is formed at the natural fracture tip and the injection pressure rises.

4. Results and Discussion

In this section, the impacts of encounter angle, in situ stress differences, elastic modulus and Poisson's ratio on fracture morphology are presented and discussed. According to the different influencing factors, the different fracturing modes of the interaction between hydraulic fracture and natural fracture are studied.

4.1. The Effect of Encounter Angle

When a hydraulic fracture intersects with a pre-existing natural fracture, the fracture propagation path is affected by the natural fracture, which is due to the low degree of bonding and lower tensile strength compared to the rock. The encounter angle of the natural fracture affects the distribution of in situ stress and the redistribution of fracturing fluid in the fracture. In order to analyze the influence of the encounter angle on fracture morphology, the fracture propagation model is established when the encounter angles of the hydraulic fracture and natural fracture are 30° , 60° and 90° , respectively. The simulation results are shown in Figure 8.

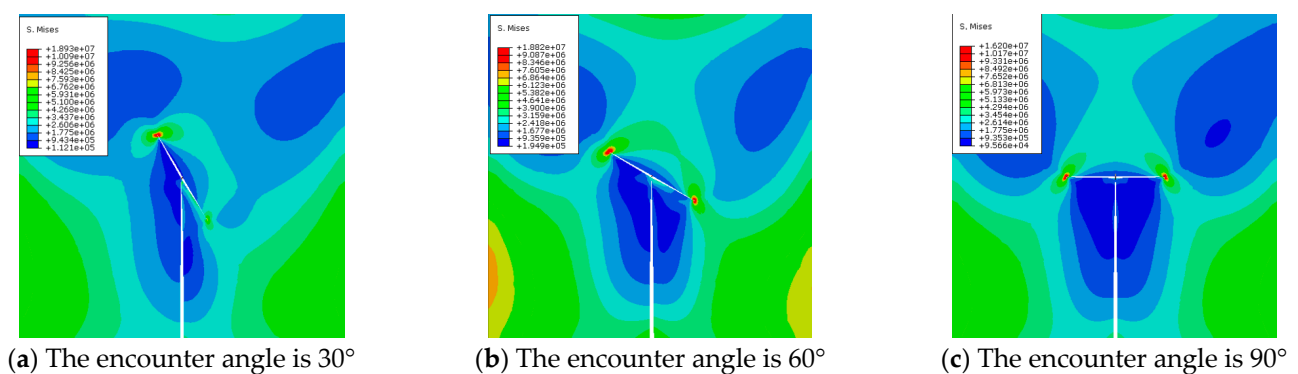


Figure 8. The fracture morphology of different encounter angles.

The hydraulic fracture intersects the natural fracture, which gradually opens with the injection of fracturing fluid [31,32]. When the encounter angles are 30° and 60° , the

natural fracture on the left opens first and forms an asymmetric stress distribution. When the encounter angle is 90° , both natural fractures open, forming a symmetrical stress distribution. The comparison between hydraulic fracture morphology and natural fracture morphology at different encounter angles is shown in Figures 9 and 10.

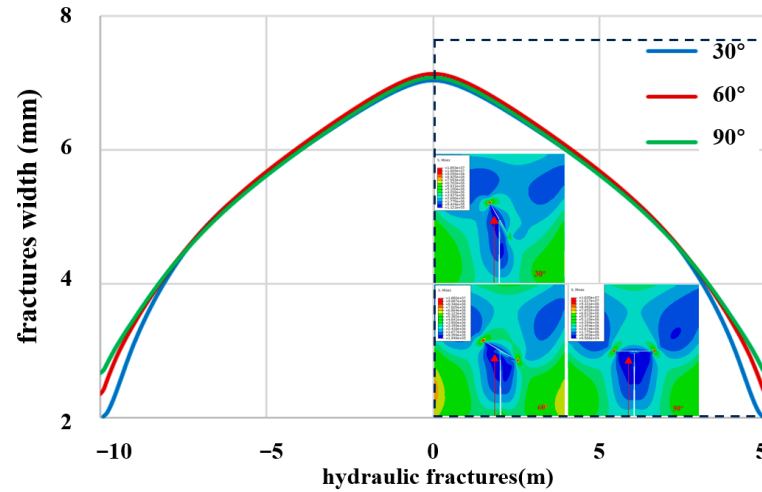


Figure 9. The hydraulic fracture morphology of natural fractures with different angles.

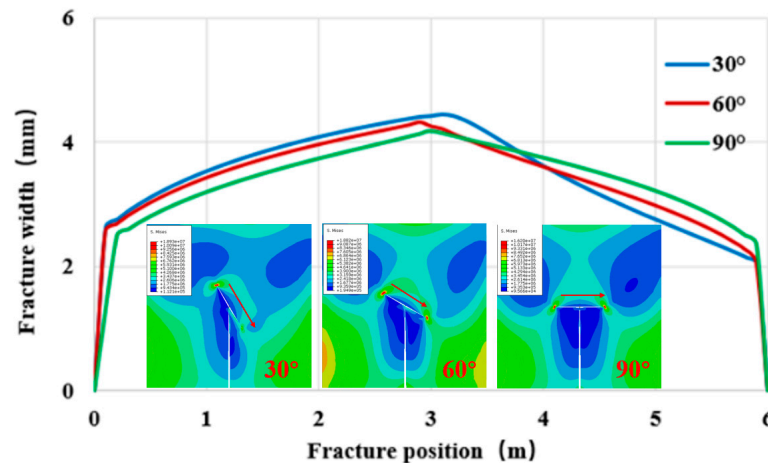


Figure 10. The natural fracture morphology of natural fractures with different angles.

As shown in Figure 9, the encounter angle has no obvious influence on the propagation form of the hydraulic fractures. When the encounter angle increases, the size of the hydraulic fractures at the injection point does not change significantly while the size of the hydraulic fractures tip becomes wider. As shown in Figure 10, when the encounter angle is 90° , natural fractures open symmetrically. When the encounter angles are 30° and 60° , the left side of the natural fracture is wider than the right side, forming asymmetrical fractures. This phenomenon can be attributed to the encounter angle's impact between natural and hydraulic fractures, which subsequently affects the redistribution of fracturing fluid flow.

4.2. The Effect of In Situ Stress Difference

The in situ stress difference has an important effect on the intersection propagation of hydraulic fractures and natural fractures [33,34]. An encounter angle of 90° was selected to analyze the influence of in situ stress differences as the fracture morphology is symmetrical. The fracture propagation models with in situ stress differences of 0 MPa, 3 MPa and 6 MPa were simulated when the encounter angle was 90° . Figure 11 illustrates the morphology of hydraulic fracture propagation when interacting with pre-existing natural fractures, considering varying in situ stress differences.

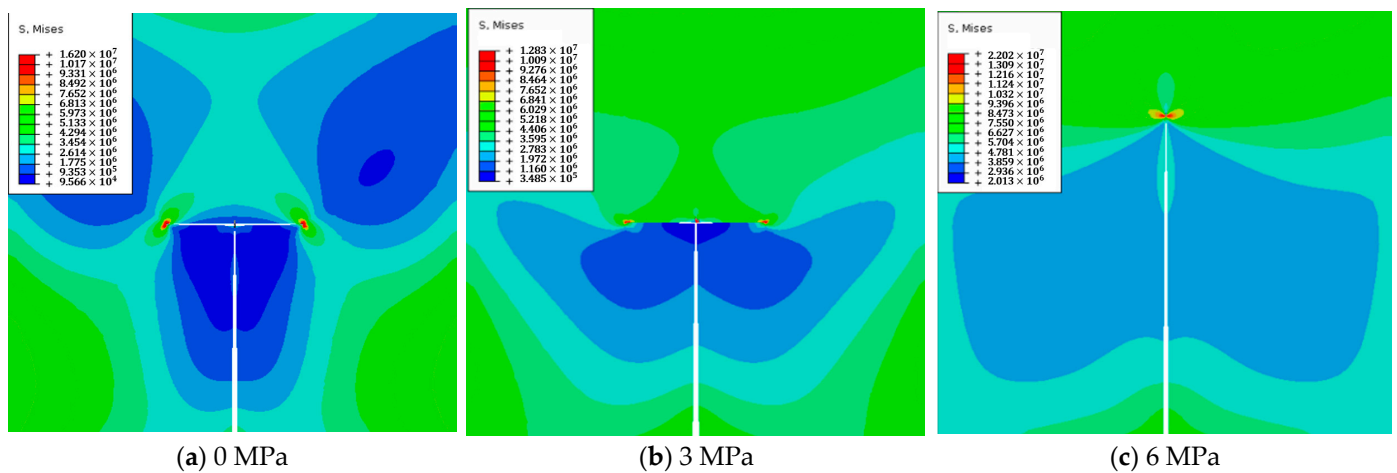


Figure 11. The fracture morphology of different in situ stress differences.

As shown in Figure 11, when the in situ stress difference is 0 MPa, the natural fracture is fully opened. The fracture is captured by the natural fracture and propagates along the natural fracture. When the stress difference is 3 MPa, the hydraulic fracture still propagates after intersecting with the natural fracture, and the stress of the fracture tip is relatively high. When the stress difference is 6 MPa, the hydraulic fracture passes through the natural fracture, and the natural fracture has no obvious influence on the propagation path of the hydraulic fracture. The fracture propagation morphology is shown in Figures 12 and 13 under different stress differences.

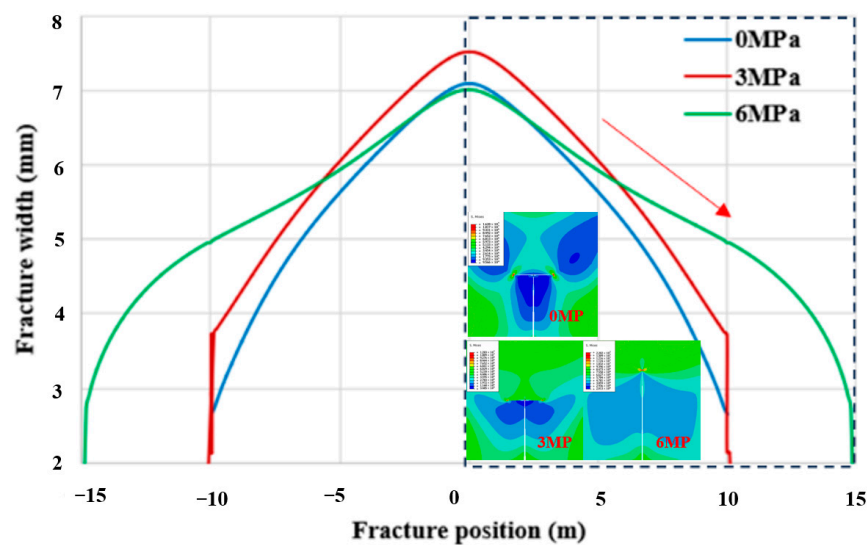


Figure 12. The hydraulic fracture morphology of different stress differences.

By comparing the fracture propagation patterns shown in Figures 12 and 13, when the in situ stress difference is 0 MPa, both hydraulic fractures and natural fractures have obvious propagation. The width of the hydraulic fracture is smaller, while the width of the natural fracture is larger. When the in situ stress difference is 3 MPa, after the hydraulic fracture intersects with the natural fracture, the artificial fracture still propagates; the width of the hydraulic fracture increases, while the width of the natural fracture is narrow. When the stress difference is 6 MPa, the propagation width of the hydraulic fracture is larger, and the natural fracture does not open. The length of the fracture continues to grow, forming a narrow and long fracture, and the natural fracture does not initiate.

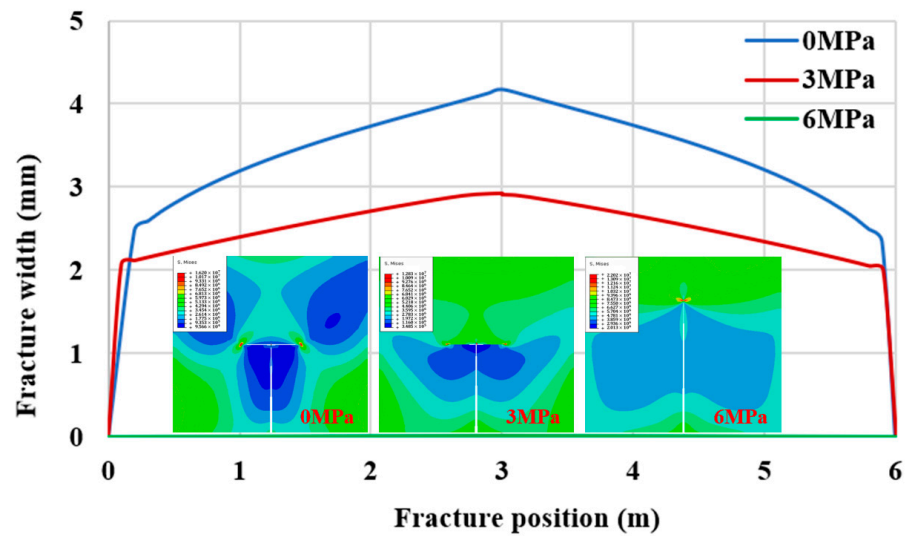


Figure 13. The natural fracture morphology of different stress differences.

4.3. The Effect of Elastic Modulus

In order to analyze the influence of elastic modulus on fracture morphology, the hydraulic fracture interaction with pre-existing natural fractures model was established, with elastic modulus values of 16 GPa, 19 GPa and 22 GPa, respectively [35]. In the models, the stress difference was 0 MPa and the Poisson's ratio was 0.3. The complex crack propagation morphology under different elastic modulus values is shown in Figure 14.

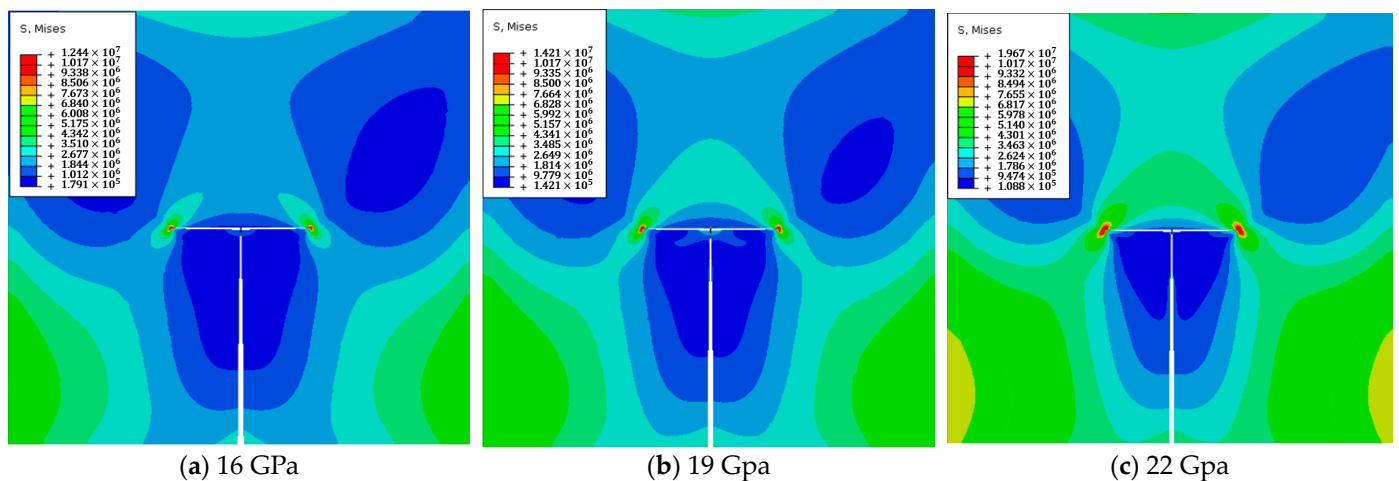


Figure 14. The fracture morphology under different elastic modulus values.

As shown in Figure 13, the fractures propagate along natural fractures in reservoirs with different elastic modulus values when the hydraulic fracture intersects with natural fractures. The stress is concentrated at the tip of the natural fracture, and the stress increases with the increase in elastic modulus. The fracture propagation morphology of the hydraulic fracture interaction with pre-existing natural fractures under different elastic modulus values is shown in Figures 15 and 16.

As shown in Figure 15, with the increase in the elastic modulus, the width of the hydraulic fracture decreases, and the width of the hydraulic fracture tip increases slightly. As can be seen from Figure 16, the opening of a natural fracture requires a lower elastic modulus, which can create a larger natural fracture width.

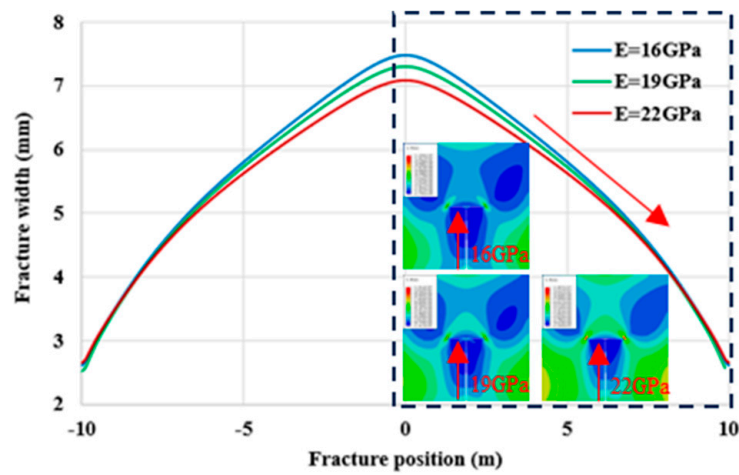


Figure 15. The hydraulic fracture morphology of different elastic modulus values.

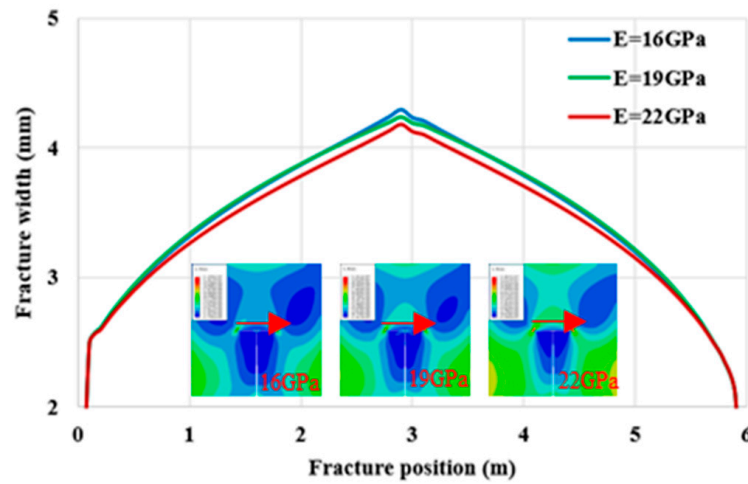


Figure 16. The natural fracture morphology of different elastic modulus values.

4.4. The Effect of Poisson's Ratio

Figure 17 shows the fracture geometry and stress distribution of different Poisson's ratios in reservoirs. The stress difference is 0 MPa. The elastic modulus is 22 GPa. The Poisson's ratios are 0.24, 0.27 and 0.3. In different models, hydraulic fractures are trapped by natural fractures and propagate along natural fractures. The Poisson's ratio has little influence on fracture morphology.

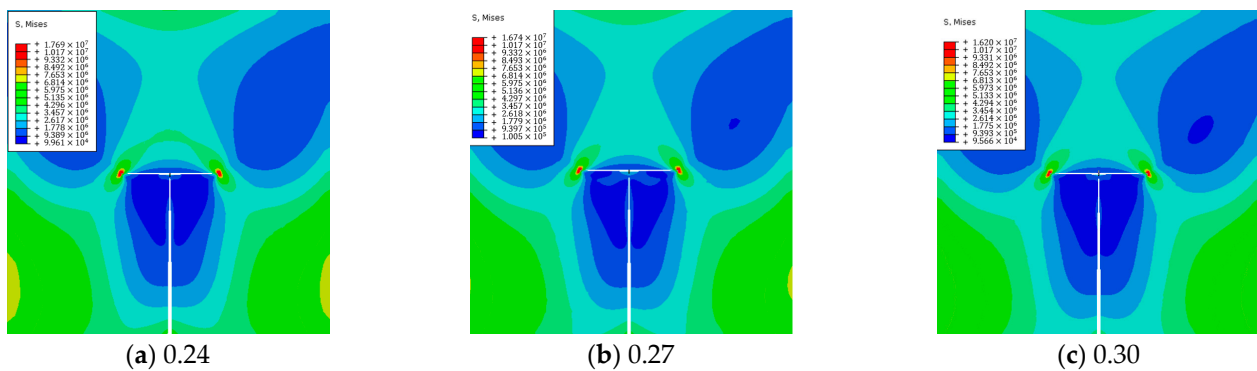


Figure 17. The fracture morphology under different Poisson's ratios.

Figure 18 shows that the width at the injection point of hydraulic fractures drops and the width at the hydraulic fracture tip grows slightly with the increase in Poisson's ratio. Figure 19 indicates that Poisson's ratio has little influence on the natural fracture propagation pattern.

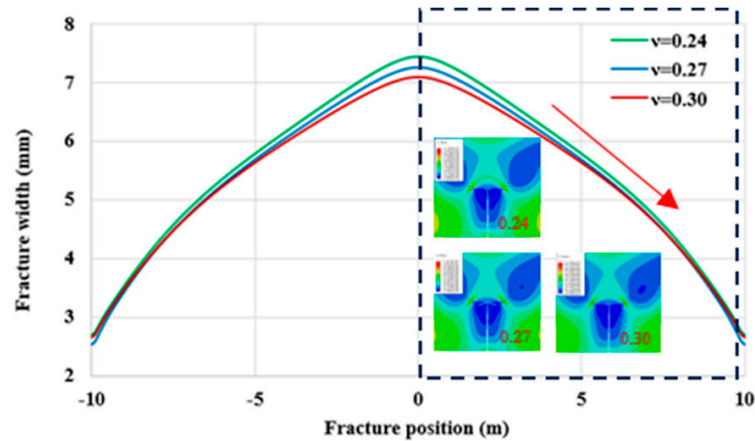


Figure 18. The hydraulic fracture morphology of different Poisson's ratios.

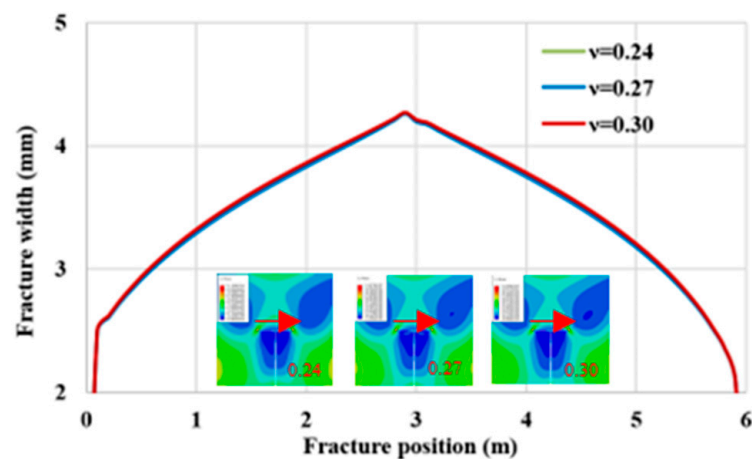


Figure 19. The natural fracture morphology of different Poisson's ratios.

4.5. The Law of Hydraulic Fracture Interaction with Pre-Existing Natural Fractures

Based on the above research, the main factors that affect the fracture propagation morphology of hydraulic fractures interacting with pre-existing single natural fractures are encounter angle and in situ stress difference [36]. The elastic modulus and Poisson's ratio have a slight influence on the fracture morphology. The propagation morphology of the hydraulic fracture interacting with pre-existing single natural fractures is analyzed by simulating the encounter angle as 15° , 30° , 45° , 60° , 75° and 90° , and the stress difference as 0 MPa, 1 MPa, 2 MPa, 3 MPa, 4 MPa, 5 MPa and 6 MPa, respectively.

Figure 20 shows that when the in situ stress difference is 0 MPa, hydraulic fractures are easy to open along both sides of the natural fractures. The fracture propagates along one side of the natural fracture when the in situ stress difference increases. The smaller the encounter angle, the more difficult it is for the fracture to pass through the natural fracture. This is due to the uneven distribution of the fracturing fluid [37]. When one side is opened, the fracture will propagate along the open channel according to the principle of minimum energy. With an increase in the in situ stress difference, the hydraulic fracture tends to propagate directly through natural fractures with high angles.

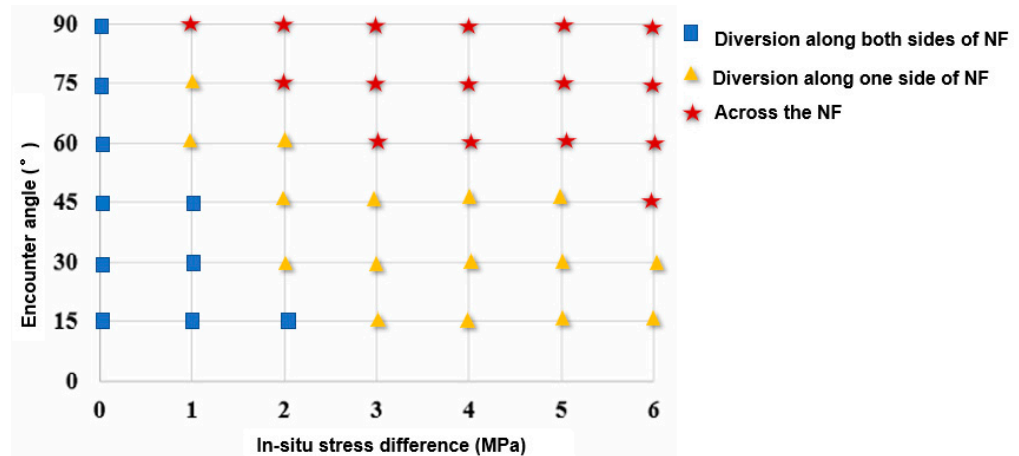


Figure 20. The propagation law of the intersection of hydraulic fractures and natural fractures.

5. Hydraulic Fracture Propagation Mechanism Intersecting with Complex Natural Fractures

The method based on the cohesive element method to analyze the intersection propagation criteria of hydraulic fractures and natural fractures has been recognized by researchers, and it is consistent with both the theoretical model and experimental results [38,39]. The natural fractures are conjugated complex natural fractures, mostly, while there was not a single fracture in fractured reservoirs. Initial natural fractures are associated with tectonic stress; however, their distribution direction may not necessarily align with the current in situ stress, as the formation may have undergone numerous tectonic events in its past. Based on the global cohesive element method, the hydraulic fracture propagation model was built, considering the complex nature fractures. Assuming that there are two conjugate fractures in the reservoir, the angle of one set of fractures will be 30° and the other will be 150° . The injection point will be located in the center of the simulated area. The fracture geometry is modeled in Figure 21.

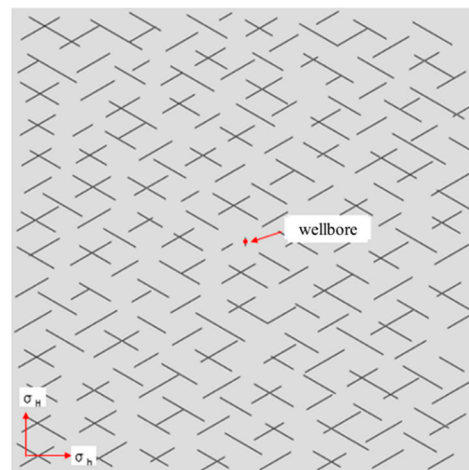


Figure 21. Geometric model.

5.1. The Effect of In Situ Stress Difference

Based on the analyzed results of fracture morphology interacting with a single fracture model, the in situ stress difference is the main factor influencing the fracture morphology [40]. Hence, the hydraulic fracture propagation processes interacting with complex natural fractures are simulated when the stress difference is 0 MPa, 2 MPa and 5 MPa. The fracture propagation morphology results are shown in Figure 22.

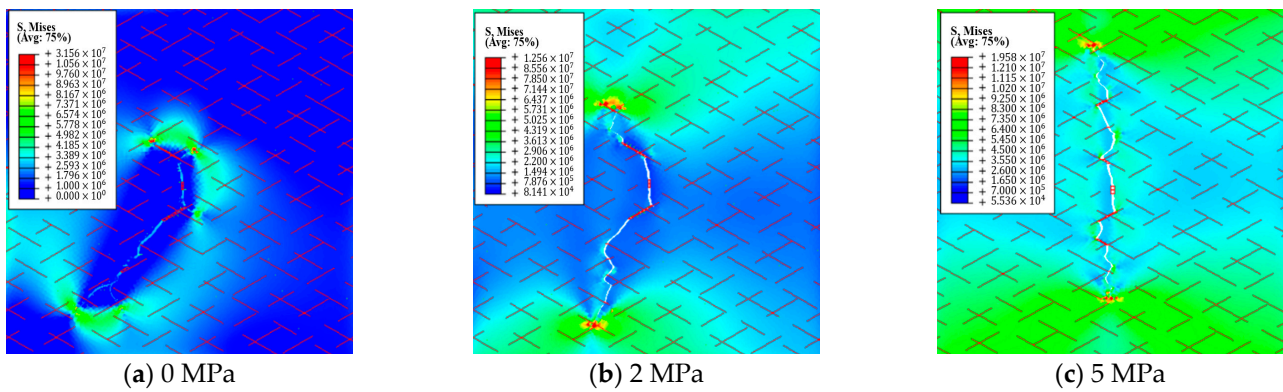


Figure 22. The fracture propagation morphology under different stress difference.

As shown in Figure 22a, the hydraulic fractures propagate along five directions. When the hydraulic fracture interacts with the natural fractures, the hydraulic fracture tends to open and propagate along natural fractures. When the stress difference is 2 MPa, the hydraulic fractures propagate along three directions. When the hydraulic fracture intersects with natural fractures, some of them traverse directly, while others propagate along the natural fractures. When the stress difference is 5 MPa, the hydraulic fracture passes through the natural fracture, and the hydraulic fracture expands along the direction of the maximum horizontal principal stress. Fracture morphology is easily affected by the distribution characteristics of natural fractures. When the stress difference is small, the formation of cracks is more complicated. The displacement of the fracture-affected area which reaches the millimeter level is larger. When the stress difference increases, the fracture propagation direction gradually becomes single. The fracture propagation direction is controlled by the direction of the maximum principal stress. The displacement of the fracture-affected area is small.

It can be seen from Figure 23 that the influence of stress difference on the fracture propagation length is slight in the random natural fracture reservoir. The maximum injection pressure is high when the stress difference increases (Figure 24). This is because the hydraulic fracture propagates and turns along more directions when the stress difference is small. This propagation pattern needs more energy.

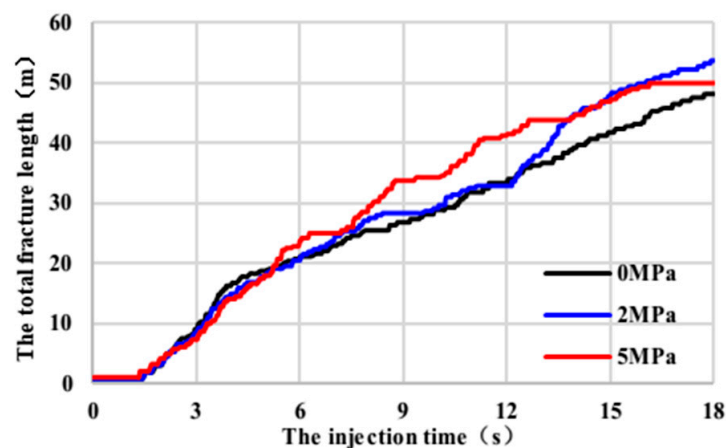


Figure 23. The fracture propagation length under different stress differences.

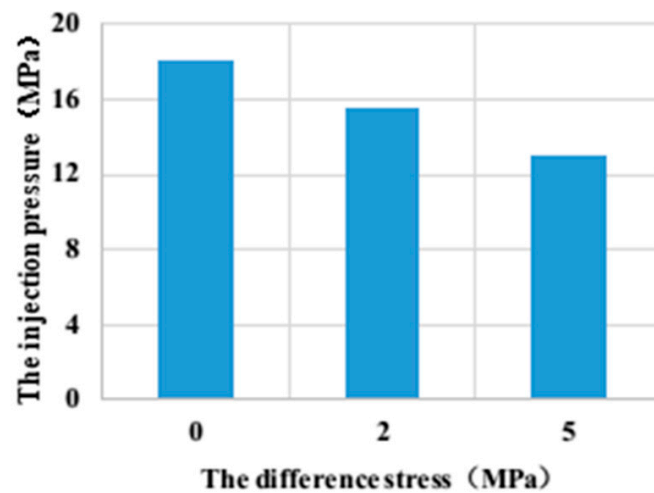


Figure 24. The injection pressure under different stress differences.

5.2. The Effect of Injection Rate

The injection rate has an important effect on fracture propagation morphology. In order to analyze the effect of injection rate on fracture propagation morphology, the fracture propagation processes are simulated when the injection rates are $0.005 \text{ m}^3/\text{s}$, $0.01 \text{ m}^3/\text{s}$ and $0.02 \text{ m}^3/\text{s}$. The total injection fluid is 0.18 m^3 for a single cluster. The fracture propagation morphology is shown in Figure 25.

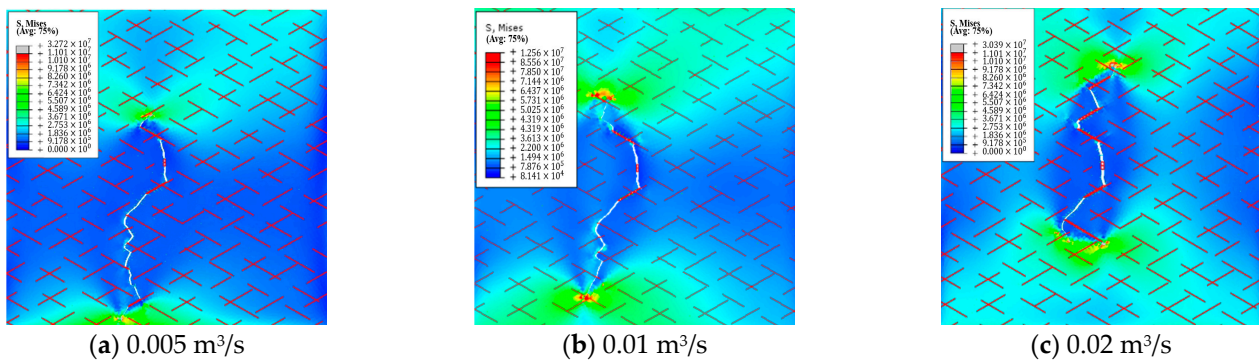


Figure 25. The fracture propagation morphology under different injection rate.

It can be seen from Figure 24 that when the injection rate is $0.005 \text{ m}^3/\text{s}$, the fracture presents asymmetric propagation morphology and the fracture deflection degree is small. When the injection rate is $0.01 \text{ m}^3/\text{s}$, the fracture propagates to both sides and displays the deflection phenomenon. When the injection rate is $0.02 \text{ m}^3/\text{s}$, the hydraulic fracture communicates the natural fracture and forms complex fractures with multiple deflections.

The comparison curves of the total fracture growth length and injection pressure under different injection rates are drawn based on the simulation results of fracture pressure growth, as shown in Figures 26 and 27, respectively.

It can be seen from Figures 26 and 27 that hydraulic fractures communicate with more natural fractures, and the fracture propagation length is long when the injection rate is large. When the injection rate is small, the fracture propagation length is short. This is due to the fact that when the injection rate is higher, the pressure in the fracture is higher, and the natural fracture is easier to open.

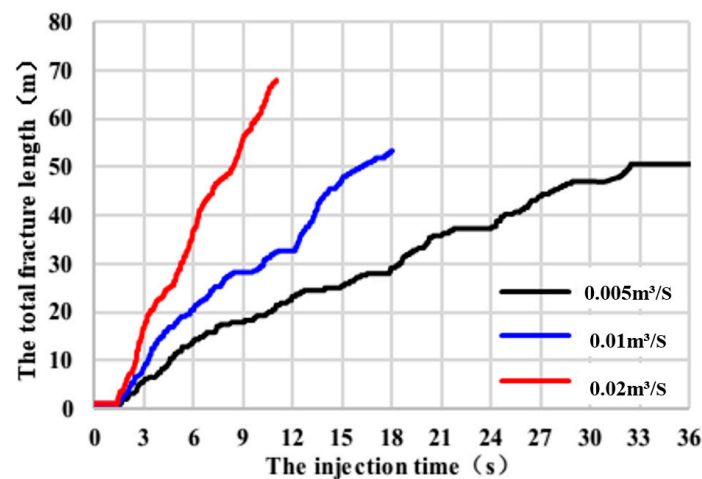


Figure 26. The fracture propagation length under different injection rates.

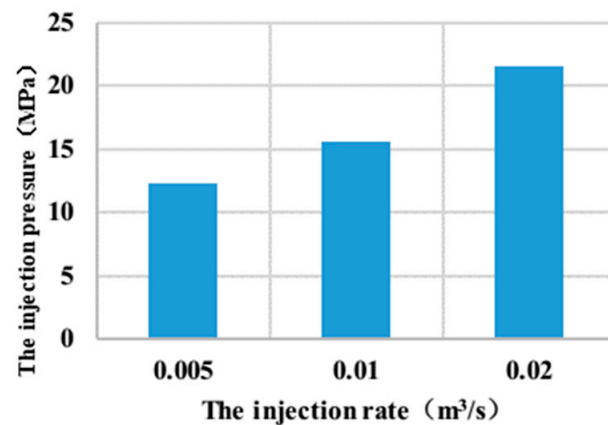


Figure 27. The injection pressure under different injection rates.

6. Conclusions

In this study, global cohesive zone methods were proposed considering fluid and solid coupling for hydraulic fracture, and the hydraulic fracture propagation law was studied. The models of hydraulic fracture interacting with pre-existing natural fractures subject to same conditions were used to probe the influences of encounter angle, stress difference, elastic modulus and Poisson's ratio on the fracture morphology. The main conclusions drawn were as follows:

- (1) The CZM is expected to be characterized for reliable fracture propagation processes, conquering the challenging problems in solving hydraulic fracture propagation interacted with pre-existing natural fractures. Based on the coupled CZM, the stress distribution and pressure variation curves of hydraulic fractures at different propagation stages were analyzed. There is an obvious stress disturbance during fracture propagation, and the injection pressure decreases significantly when it meets with natural fractures.
- (2) When the encounter angle is small, it is easy to propagate along natural fractures and form asymmetrical fracture widths. Hydraulic fractures tend to spread along natural fractures when the in situ stress difference is small, and hydraulic fractures tend to pass through natural fractures when the local stress difference is large. When the elastic modulus is small, it is beneficial to the propagation of hydraulic fractures and natural fractures. The Poisson's ratio has a slight effect on the fracture propagation pattern. The low in situ stress and low natural angle facilitate the opening of natural fractures.
- (3) A dynamic model of hydraulic fracture propagation with random natural fracture is established. When the hydraulic fracture intersects with complex natural fractures, there are multiple intersects such as capture and pass through. When the stress

difference is small, the fracture morphology formed by hydraulic fractures is more complex and the injection pressure is higher.

- (4) A hydraulic fracture propagation model with complex natural fractures in the reservoir was established. When the stress difference is small, the hydraulic fractures communicate with more natural fractures and form more complex fractures. When the injection rate is larger, the pressure in the fracture is higher, and it is easy to open natural fractures and for complex fractures to be formed.

Tight sandstone reservoirs are rich in oil and gas resources. For tight sandstone reservoirs with natural fractures, the design of the hydraulic fracturing scheme can be refined based on rock mechanics parameters and the distribution of natural fractures, as well as the distribution of the remaining oil in the reservoir. This model can provide a development idea for similar reservoirs. In the future, the complex distribution of natural fractures should be considered for further study.

Author Contributions: Methodology, S.L. and L.Q.; Software, H.Z.; Validation, H.Z., J.W. and L.Q.; Investigation, X.X.; Data curation, L.Z.; Writing—original draft, S.L. and H.Z.; Writing—review & editing, S.L.; Visualization, Y.L.; Project administration, S.L.; Funding acquisition, H.Z. All authors have read and agreed to the published version of the manuscript.

Funding: This research was financially supported by the National Natural Science Foundation of China (No. 52274005); the National Foundation Cultivation Fund Project of Northeast Petroleum University (2022GPL-10); and the Talent Introduction and Research Start-Up Fund of Northeast Petroleum University (13051202008).

Data Availability Statement: Data are contained within the article.

Conflicts of Interest: Author Qin Lan is employed by the company Petrochina Southwest Oil and Gas Field Company. The remaining authors declare that the research was conducted in the absence of any commercial or financial relationships that could be construed as a potential conflict of interest.

References

- Rahman, M.M.; Rahman, S.S. Studies of Hydraulic Fracture-Propagation Behavior in Presence of Natural Fractures: Fully Coupled Fractured-Reservoir Modeling in Poroelastic Environments. *Int. J. Geomech.* **2013**, *13*, 809–826. [[CrossRef](#)]
- Wang, F.; Xu, H.; Liu, Y.; Meng, X.; Liu, L. Mechanism of Low Chemical Agent Adsorption by High Pressure for Hydraulic Fracturing-Assisted Oil Displacement Technology: A Study of Molecular Dynamics Combined with Laboratory Experiments. *Langmuir* **2023**, *39*, 16628–16636. [[CrossRef](#)] [[PubMed](#)]
- Tan, P.; Chen, Z.; Fu, S.; Zhao, Q. Experimental investigation on fracture growth for integrated hydraulic fracturing in multiple gas bearing formations. *Geoenergy Sci. Eng.* **2023**, *231*, 212316. [[CrossRef](#)]
- Gale, J.F.W.; Reed, R.M.; Holder, J. Natural fractures in the Barnett Shale and their importance for hydraulic fracture treatments. *AAPG Bull.* **2007**, *91*, 603–622. [[CrossRef](#)]
- Tan, P.; Jin, Y.; Pang, H. Hydraulic fracture vertical propagation behavior in transversely isotropic layered shale formation with transition zone using XFEM-based CZM method. *Eng. Fract. Mech.* **2021**, *248*, 107707. [[CrossRef](#)]
- Tan, P.; Pang, H.; Zhang, R.; Jin, Y.; Zhou, Y.; Kao, J.; Fan, M. Experimental investigation into hydraulic fracture geometry and proppant migration characteristics for southeastern Sichuan deep shale reservoirs. *J. Pet. Sci. Eng.* **2020**, *184*, 106517. [[CrossRef](#)]
- Jiang, M.Z.; Zhao, G.F.; Bai, N.Y.; Zhang, S.R. Research on the law of hydraulic fracture and natural fracture intersecting extension in the heterogeneous fractured reservoir. *J. Chem. Pharm. Res.* **2014**, *6*, 816–820.
- Inglis, C.E. Stress in a plate due to the presence of cracks and sharp corners. *trans. Inst. Nav. Arch.* **1913**, *55*, 219.
- Aliha, M.R.M.; Hosseinpour, G.R.; Ayatollahi, M.R. Application of cracked triangular specimen subjected to three-point bending for investigating fracture behavior of rock materials. *Rock Mech. Rock Eng.* **2013**, *46*, 1023–1034. [[CrossRef](#)]
- Aliha, M.; Bahmani, A.; Akhondi, S. Numerical analysis of a new mixed mode I/III fracture test specimen. *Eng. Fract. Mech.* **2015**, *134*, 95–110. [[CrossRef](#)]
- Ayatollahi, M.R.; Saboori, B. Maximum tangential strain energy density criterion for general mixed mode I/II/III brittle fracture. *Int. J. Damage Mech.* **2015**, *24*, 263–278. [[CrossRef](#)]
- Yao, Y. Linear elastic and cohesive fracture analysis to model hydraulic fracture in brittle and ductile rocks. *Rock Mech. Rock Eng.* **2012**, *45*, 375–387. [[CrossRef](#)]
- Deng, S.; Zhu, Z.M.; Wang, L. Study on the influence of in-situ stresses on dynamic fracture behaviors of cracks. *Chin. J. Rock Mech. Eng.* **2019**, *38*, 1989–1999.
- Zhang, S.C.; Guo, T.K.; Zhou, T.; Zou, Y.; Mu, S. Fracture propagation mechanism experiment of hydraulic fracturing in natural shale. *Acta Pet. Sin.* **2014**, *35*, 496–503.

15. Hou, B.; Tan, P.; Chen, M.; Yuan, L.; Xiong, Z.Y.; Xu, C.L. Experimental investigation on propagation geometry of hydraulic fracture in compact limestone reservoirs. *Chin. J. Rock Mech. Eng.* **2016**, *38*, 219–225.
16. Hui, G.; Chen, Z.; Schultz, R.; Chen, S.; Song, Z.; Zhang, Z.; Song, Y.; Wang, H.; Wang, M.; Gu, F. Intricate unconventional fracture networks provide fluid diffusion pathways to reactivate pre-existing faults in unconventional reservoirs. *Energy* **2023**, *282*, 128803. [[CrossRef](#)]
17. Kar, S.; Chaudhuri, A.; Singh, A.; Pal, S. Phase field method to model hydraulic fracturing in saturated porous reservoir with natural fractures. *Eng. Fract. Mech.* **2023**, *286*, 109289. [[CrossRef](#)]
18. Cundall, P.A.; Strack, O.D. A discrete numerical model for granular assemblies. *Geotechnique* **1979**, *29*, 47–65. [[CrossRef](#)]
19. Cottrell, M.; Hosseinpour, H.; Dershowitz, W. Rapid discrete fracture analysis of hydraulic fracture development in naturally fractured reservoirs. In Proceedings of the SPE/AAPG/SEG Unconventional Resources Technology Conference, Denver, CO, USA, 12–14 August 2013.
20. Xia, L.; Zeng, Y.W.; Jin, L. Research on influence of initial horizontal principal stress on stress shadow. *Chin. J. Rock Mech. Eng.* **2016**, *1*, 2819–2825.
21. Fatahi, H.; Hossain, M.; Sarmadivaleh, M. Numerical and experimental investigation of the interaction of natural and propagated hydraulic fracture. *J. Nat. Gas Sci. Eng.* **2017**, *37*, 409–424. [[CrossRef](#)]
22. Song, X.; Liu, H.; Zheng, X. Numerical simulation of hydraulic fracture propagation in fractured reservoir using global cohesive zone method. *Front. Phys.* **2023**, *11*, 1272563. [[CrossRef](#)]
23. Rueda, J.; Mejia, C.; Roehl, D. 3D unrestricted fluid-driven fracture propagation based on coupled hydromechanical interface elements. *Eng. Fract. Mech.* **2022**, *272*, 108680. [[CrossRef](#)]
24. Chen, Z.; Bungler, A.; Zhang, X.; Jeffrey, R.G. Cohesive zone finite element based modeling of hydraulic fractures. *Acta Mech. Solida Sin.* **2009**, *22*, 443–452. [[CrossRef](#)]
25. Li, S.; Chen, Z.; Li, W.; Yan, T.; Bi, F.; Tong, Y. An FE Simulation of the Fracture Characteristics of Blunt Rock Indenter under Static and Harmonic Dynamic Loadings using Cohesive Elements. *Rock Mech. Rock Eng.* **2023**, *56*, 2935–2947. [[CrossRef](#)]
26. Guo, J.; Zhao, X.; Zhu, H.; Zhang, X.; Pan, R. Numerical simulation of interaction of hydraulic fracture and natural fracture based on the cohesive zone finite element method. *J. Nat. Gas Sci. Eng.* **2015**, *25*, 180–188. [[CrossRef](#)]
27. Guo, J.; Luo, B.; Lu, C.; Lai, J.; Ren, J. Numerical Investigation of Hydraulic Fracture Propagation in a Layered Reservoir using the Cohesive Zone Method. *Eng. Fract. Mech.* **2017**, *186*, 195–207. [[CrossRef](#)]
28. Zhou, Y.; Guan, W.; Cong, P.; Sun, Q. Effects of heterogeneous pore closure on the permeability of coal involving adsorption-induced swelling: A micro pore-scale simulation. *Energy* **2022**, *258*, 124859. [[CrossRef](#)]
29. Zhang, X.; Jeffrey, R.G. The role of friction and secondary flaws on deflection and re-initiation of hydraulic fractures at orthogonal pre-existing fractures. *Geophys. J. R. Astron. Soc.* **2010**, *167*, 1454–1465. [[CrossRef](#)]
30. Zhou, T.; Wang, H.; Li, F.; He, B.; Zhou, T.; Li, N. Influence mechanism of fracturing fluid filtration on fracture initiation and dynamic closure process. *Nat. Gas Ind.* **2023**, *43*, 91–101.
31. Chen, J.; Yang, R.; Qin, X.; Huang, Z.; Jing, M.; Li, J.; Li, G. Mechanism of stress-permeability evolution in fan-shaped cavity completion of coalbed methane horizontal wells. *Nat. Gas Ind.* **2024**, *44*, 184–198.
32. Kong, X.; Yan, R.; Zhang, S.; Yuan, Q.; Chen, Q.; Xu, H. Simulation experiment of fracture initiation and propagation of hydraulic fracturing with true triaxial large physical model. *Chem. Eng. Oil Gas* **2023**, *52*, 97–102.
33. Hao, Y.; Liu, J.; Wu, L.; Zhou, X.; Li, J.; Jiang, Y. Natural fractures in the Longmaxi Formation, Weiyuan block: Characteristics, distribution patterns and forming episodes. *Nat. Gas Technol. Econ.* **2024**, *18*, 23–31.
34. Li, Y.; Yang, Y.; Wang, A.; Dai, L. Fracture propagation model accounting for intersection among hydraulic fractures and natural fractures in three-dimensional space. *J. China Coal Soc.* **2024**, 1–11.
35. Zeng, L.; Gong, L.; Su, X.; Mao, Z. Natural fractures in deep to ultra-deep tight reservoirs: Distribution and development. *Oil Gas Geol.* **2024**, *45*, 1–14.
36. He, Q.; Zhong, Z.; Alabboodi, M.; Wang, G. Artificial Intelligence Assisted Hydraulic Fracturing Design in Shale Gas Reservoir. In Proceedings of the SPE Eastern Regional Meeting, Charleston, WV, USA, 15–17 October 2019; pp. 15–17.
37. Liu, Z.; Pan, Z.; Li, S.; Zhang, L.; Wang, F.; Han, L.; Zhang, J.; Ma, Y.; Li, H.; Li, W. Study on the effect of cemented natural fractures on hydraulic fracture propagation in volcanic reservoirs. *Energy* **2022**, *241*, 122845. [[CrossRef](#)]
38. Chen, Z.; Jeffrey, R.G.; Zhang, X.; Kear, J. Finite-element simulation of a hydraulic fracture interacting with a natural fracture. *SPE J.* **2017**, *22*, 219–234. [[CrossRef](#)]
39. Yin, S.; Zhao, J.; Liu, P.; Shen, Z.; Zhou, Y.; He, Z. Evaluation of opening and extension conditions of natural and hydraulic fractures in fractured reservoir. *Pet. Drill. Tech.* **2024**, 1–14.
40. Wei, H. Research progress on fracture propagation patterns of hydraulic fracturing in heterogeneous shale. *Pet. Geol. Recovery Effic.* **2023**, *30*, 156–166. [[CrossRef](#)]

Disclaimer/Publisher’s Note: The statements, opinions and data contained in all publications are solely those of the individual author(s) and contributor(s) and not of MDPI and/or the editor(s). MDPI and/or the editor(s) disclaim responsibility for any injury to people or property resulting from any ideas, methods, instructions or products referred to in the content.